scientific reports

Check for updates

OPEN

DFT investigation of iron-doped boron nitride nanoparticles for anastrozole drug delivery and molecular interaction

Mohammad J. Akbar[1]✉, Adil Farooq Wali[2], Sirajunisa Talath[2], Abdullah Aljasser[1], Mohammed M. Aldurdunji[3], Fahad Alqahtani[4], Sathvik B. Sridhar[2], M. Yasmin Begum[5] & Umme Hani[5]

The development of efficient drug delivery systems is critical for improving therapeutic outcomes and reducing side effects in cancer treatment. This study investigates the potential of iron-doped boron nitride nanoparticles (Fe-BNNPs) as a nanocarrier for Anastrozole, a key aromatase inhibitor used in breast cancer therapy. Using density functional theory (DFT), we systematically analyzed the interaction mechanisms between Anastrozole and Fe-BNNPs, focusing on binding energies, electronic properties, and structural stability. Our results reveal a strong adsorption of Anastrozole on Fe-BNNPs, with binding energies ranging from − 0.6 to − 1.4 eV, indicating a stable and efficient drug-carrier interaction. Iron doping significantly enhances the reactivity of BNNPs, improving drug loading and release capabilities. Nanoparticles passivated with -H and -OH groups and functionalized with iron nanoclusters were examined, demonstrating that -H passivation yields more stable structures compared to -OH, despite minor variations in electronic properties such as energy gaps (e.g., 2.51 eV for -H vs. 2.54 eV for -OH). The incorporation of iron nanoclusters further increases the binding energy of Anastrozole by approximately 40%, highlighting its role in optimizing drug-nanocarrier interactions. Optical absorption spectra reveal distinct peaks for Anastrozole adsorption on -H and -OH passivated surfaces, providing a clear indicator of interaction states. These findings underscore the potential of Fe-BNNPs as a promising nanocarrier for targeted Anastrozole delivery, offering enhanced precision and therapeutic efficacy.

Keywords DFT, Anastrozole, BN nanoparticles, Drug delivery

The search for effective drug delivery systems has become a major focus in the field of nanomedicine, particularly in cancer treatment. Traditional chemotherapy often faces challenges such as poor solubility, nonspecific targeting, and systemic toxicity, which can result in significant adverse effects for patients. Consequently, the development of nanocarrier that can enhance the delivery and effectiveness of anticancer drugs is of paramount importance. Among various nanomaterials, boron nitride nanoparticles (BNNPs) have emerged as promising candidates due to their unique properties, including high thermal and chemical stability, biocompatibility, and excellent mechanical strength[1,2]. In recent years, the incorporation of dopants into BNNPs has been explored to enhance their performance. Iron, in particular, has garnered attention due to its magnetic properties and its ability to improve the electronic properties of BNNPs, thereby facilitating drug loading and release mechanisms[3,4]. Merlo et al.[5] conducted a comprehensive review of boron nitride nanomaterials, emphasizing their excellent biocompatibility and potential for bio-applications. The study concluded that BN nanomaterials exhibit low toxicity and are suitable for use in biomedical contexts, including drug delivery systems. Wang et al.[6] synthesized Fe_3O_4 nanoparticle-coated boron nitride nanospheres and performed detailed biocompatibility studies. Their results demonstrated that the hybrid nanostructures exhibited no significant cytotoxicity and

[1]Department of Pharmaceutics, College of Clinical Pharmacy, Imam Abdulrahman Bin Faisal University, P.O. Box 1982, Dammam 31441, Saudi Arabia. [2]RAK College of Pharmacy, RAK Medical & Health Sciences University, Ras Al Khaimah, United Arab Emirates. [3]Pharmaceutical Practices Department, College of Pharmacy, Umm Al-Qura University, Makkah, Saudi Arabia. [4]Department of Pharmaceutical Sciences, College of Pharmacy, Umm Al-Qura University, Makkah, Saudi Arabia. [5]Department of Pharmaceutics, College of Pharmacy, King Khalid University, Abha, Saudi Arabia. ✉email: mjakbar@iau.edu.sa

maintained good biocompatibility, further supporting their potential for biomedical applications. Fe-doped boron nitride nanoparticles (Fe-BNNPs) not only maintain the structural integrity of the BN framework but also exhibit increased reactivity, rendering them suitable carriers for drug molecules[7,8]. The interaction between Anastrozole and nanocarriers such as Fe-BNNPs can influence the pharmacokinetics and pharmacodynamics of the drug, thereby enhancing therapeutic efficacy while minimizing side effects[9,10]. Anastrozole, a potent aromatase inhibitor, plays a crucial role in treating estrogen receptor-positive breast cancer, especially in postmenopausal women[11]. Despite its efficacy, limitations in distribution and bioavailability necessitate innovative delivery systems to optimize therapeutic outcomes[12,13]. Iron doping modifies the electronic structure and surface properties of nanoparticles, enhancing their adsorption capacity and reactivity. This modification is particularly advantageous for achieving higher drug concentrations at tumor sites, which is essential for effective cancer treatment. Additionally, the magnetic properties introduced by iron doping enable targeted delivery through external magnetic fields, allowing precise localization of the drug carrier to tumor sites. This capability minimizes systemic side effects and improves the therapeutic index of Anastrozole, representing a significant advancement over conventional delivery systems[14].

Density functional theory (DFT) has become a valuable tool for investigating interactions between drug molecules and nanocarriers at the atomic level. DFT calculations enable the analysis of binding energies, electronic properties, and structural stabilities, offering insights into the mechanisms governing drug loading and release[15–18]. Recent studies utilizing DFT have demonstrated that the electronic structure of nanocarriers can be significantly altered through doping, enhancing their ability to bind and efficiently release drug molecules[19–22]. Beyond structural properties, the surface chemistry of Fe-BNNPs plays a pivotal role in their interaction with Anastrozole. Surface functionalization strategies can enhance the loading capacity and stability of drugs on the nanocarrier surface. Various chemical modifications on the surface of BNNPs can enhance their dispersion in biological environments and facilitate more effective drug delivery[23]. Therefore, understanding the surface interactions between Anastrozole and Fe-BNNPs is crucial to optimize their application in targeted therapy. Additionally, the size and morphology of nanocarriers play a significant role in their performance in drug delivery. Smaller nanoparticles often exhibit better cellular uptake, while larger nanoparticles can offer sustained drug release. The design of Fe-BNNPs can be customized to achieve the optimal size and shape for specific therapeutic applications, thereby increasing the overall efficiency of the drug delivery system[24].

Another important consideration is the potential use of magnetic fields to control the transport of drugs loaded on Fe-BNNPs. The magnetic properties of iron-doped nanoparticles enable targeted delivery through external magnetic fields, allowing precise drug localization at the tumor site. This approach not only enhances the therapeutic index of Anastrozole but also reduces systemic exposure and associated side effects[25,26]. Moreover, the biocompatibility of Fe-BNNPs is a critical factor in their application as drug carriers. Cytotoxicity assessment of these nanomaterials is essential to ensure their safety in clinical settings. Recent studies have shown promising results regarding the biocompatibility of BN-based nanomaterials, suggesting their effective utilization in biological systems without significant adverse effects[27]. The stability of drug-nanocarrier complexes is another crucial parameter that impacts the effectiveness of drug delivery systems. Environmental factors such as pH, temperature, and ionic strength can influence the stability and release profile of the drug. By optimizing the conditions for loading Anastrozole onto Fe-BNNPs, enhanced stability and controlled release can be achieved, further improving therapeutic outcomes[28]. Furthermore, besides enhancing drug delivery, the use of Fe-BNNPs can facilitate imaging and monitoring of therapeutic efficacy. The magnetic properties of iron can be utilized for magnetic resonance imaging (MRI), offering a non-invasive means to track drug distribution within the body. This dual functionality of Fe-BNNPs as both drug carriers and imaging agents can significantly advance personalized medicine approaches in cancer treatment[29]. The integration of computational modeling and experimental validation is crucial for the successful development of Fe-BNNPs as drug delivery systems. Computational studies, such as those conducted using DFT, can inform the design of nanocarriers by predicting their interactions with drug molecules. Validation through experimental techniques, including spectroscopy and microscopy, can validate these predictions and offer insights into the real-world behavior of nanocarriers[30]. As the field of nanomedicine progresses, the discovery of multifunctional nanocarriers like BNNPs becomes increasingly vital. The capacity to load multiple therapeutic agents, regulate their release, and monitor their distribution opens up new possibilities for combination therapies in cancer treatment. This approach can generate synergistic effects that enhance therapeutic efficacy while mitigating potential resistance mechanisms[18,31–33]. Exploring iron-doped boron nitride nanoparticles as carriers of Anastrozole presents a promising avenue for enhancing drug delivery systems in oncology. By combining theoretical insights from DFT with experimental methodologies, this study aims to establish a comprehensive understanding of the interactions between Anastrozole and Fe-BNNPs. These discoveries are anticipated to aid in the development of more efficient and targeted drug delivery strategies, ultimately enhancing patient outcomes in cancer treatment. Furthermore, this study bridges a critical gap in the literature by employing DFT to investigate the binding mechanisms and stability of Anastrozole on Fe-BNNCs. While boron nitride nanomaterials have been widely studied, the specific interactions between Anastrozole and Fe-BNNCs have not been thoroughly explored. By combining computational modeling with experimental insights, this research provides a comprehensive understanding of the drug-carrier interaction, paving the way for the development of more efficient and targeted nanocarriers in oncology.

Computational details

In this research, DFT-based computational methods were employed to explore the binding energy of Anastrozole to iron-modified boron nitride nanoparticles (Fe-BNNPs) and to analyze the optical properties of the most stable configurations of Anastrozole bound to Fe-BNNPs. The methodology encompassed the utilization of the TurboMole code[34] for density functional theory (DFT) computations, DFTB + for optimized DFT calculations[35],

and the Ab-initio OpenMX simulation package[36] for additional assessments and measurements of optical properties. For the treatment of nanoparticles, the cluster method was utilized, and k-point sampling was conducted at the gamma point of the Brillouin zone. The combined PBE functional, along with an appropriate basis set like def2-TZVP[37], was utilized to comprehensively describe the electronic structure of the systems. The initial coordinates of Fe-BNNPs and Anastrozole were optimized to determine the conformations with the lowest energy. Convergence criteria were established with a maximum force threshold of 0.001 eV/Å. To address the matching error of the BSSE basis set, an inverse correction approach was employed, following the established method by Boys and Bernardi[38], to rectify the BSSE in all absorption energy calculations. This strategy effectively mitigates the overestimation of interaction energies stemming from incomplete basis sets. The BSSE correction was consistently integrated into the interaction energies within the binding energy formula.

The binding energy (E_{bind}) of Anastrozole on the Fe-BNNP surface was computed using the following equation:

$$E_{bind}=E_{BNNC@AN}-(E_{AN}+E_{BNNC})+E_{BSSE} \quad (1)$$

where $E_{BNNC@AN}$ is the total energy of the Anastrozole-Fe-BNNP complex, E_{BNNC} represents the energy of the nanocrystal, and E_{AN} denotes the energy of the drug molecule. In Eq. 1, E_{bind} signifies the total energy of the system, and E_{BSSE} is the correction applied to the Basis Set Superposition Error (BSSE). It is essential to compute the zero-point energy (ZPE)[39] values for the system and its constituent elements to correctly adjust the binding energy as follows:

$$E_{bind}^{corrected} = E_{bind} + \left(E_{ZPE}^{BNNC@AN} - E_{ZPE}^{AN} - E_{ZPE}^{BNNC}\right) \quad (2)$$

The initial optimization was conducted utilizing the DFTB + method. DFTB parameters were chosen in alignment with the existing Slater-Koster tables for boron and iron nitride[40], guaranteeing compatibility with DFT outcomes. Following a methodology akin to DFT, the geometry of the complexes was further fine-tuned using DFTB + to expedite computations without compromising precision. Subsequent recalculations of binding energies were executed, accompanied by a charge density analysis to elucidate the electronic interactions between anastrozole and Fe-BNNP. To ensure precise calculations, a plane wave cutoff energy of 500 eV was set in place.

Results and discussion

Figure 1 illustrates BN nanoparticles coated with hydrogen atoms, showcasing nanoparticles with approximate radii of 3, 5, 7, and 9 Å. In the bulk structure, the B-N bond length extends around 1.56 Å, yet in nanoparticles, this distance diminishes to a range of 1.42 to 1.48 Å from the core to the surface. Notably, the B-N bond length decreases prominently as one approaches the surface, influenced by the heightened surface-to-volume ratio in smaller nanoparticles. This augmentation in surface area prompts alterations in electron distribution and atomic bonding, culminating in the reduction of the B-N bond length[41].

N-H and B-H bonds are prevalent on the nanoparticle surface, with bond lengths spanning from 1.08 to 1.12 Å, respectively. The IR spectrum of BN nanocrystal samples exhibits peaks at 670, 730, 810, 950, 1030, and 1115, along with additional peaks at 1240 and 1469 cm^{-1}, aligning with experimental findings[42]. In Table 1 we have shown the comparison of DFT results with published experimental and theoretical Data.

Surface hydrogen bonds bolster the chemical stability of nanoparticles, which is also contingent upon various structural attributes. The formation energy of B-N nanoparticles coated with hydrogen is size-dependent, with values for structures of 3, 5, 7, and 9 Å gauging at -13.4, -3.76, -3.21, and − 2.93 eV/atom, respectively. The stability of BN nanoparticles holds paramount significance in their utility as drug carriers, underscoring the pivotal role of surface modifications despite the potential drastic alterations in nanocrystal properties.

Functionalizing BN boron nitride nanoparticles with -OH hydroxyl groups mark a substantial advancement in nanomaterial science[46]. The introduction of -OH groups amplify the chemical reactivity and surface characteristics of BN nanoparticles, rendering them versatile for diverse applications in electronics, catalysis, and biomedicine[47]. Functionalization enhances the dispersibility of BN nanoparticles in polar solvents, facilitates their integration into composite materials, and augments overall performance levels[48].

In catalysis, functionalized BN nanoparticles serve as valuable support materials owing to their expansive surface area and modifiable surface chemistry. The presence of -OH groups can enhance the adsorption of catalytic species or reactants, thereby elevating catalytic activity. Also, functionalization plays a pivotal role in stabilizing active sites, consequently prolonging the lifespan and enhancing the reusability of the catalyst[49]. Moreover, in biomedicine, BN nanoparticles functionalized with -OH groups exhibit promise as potent drug delivery systems and imaging agents. The hydrophilic nature of hydroxyl groups bolsters biocompatibility and fosters improved interactions with biological molecules. This functionalization enhances the solubility of BN nanoparticles in biological milieus, facilitating cellular absorption. Consequently, they find utility in targeted drug delivery applications and as contrast agents in medical imaging modalities, leveraging their distinctive optical and thermal characteristics[50].

The functionalization of BN nanoparticles with -OH groups markedly influences their mechanical and thermal properties. Such modifications can engender enhanced stability and resistance to oxidation, crucial for sustaining performance in challenging environments. Furthermore, the presence of hydroxyl groups has the potential to induce alterations in the network structure and bonding properties of BN, potentially augmenting mechanical strength and thermal conductivity[51]. Figure 2 depicts BN nanoparticles enveloped with -OH groups, featuring B-N, N-O, and B-O bond lengths ranging from 1.45 to 1.49 Å. The formation energy of (BN)-OH nanoparticles, with sizes 3, 5, 7, and 9 Å, approximates − 2.28, -2.01, -1.81, and − 1.39 eV/atom, significantly lower than that of (BN)-H nanoparticles. The negative formation energy underscores their structural stability,

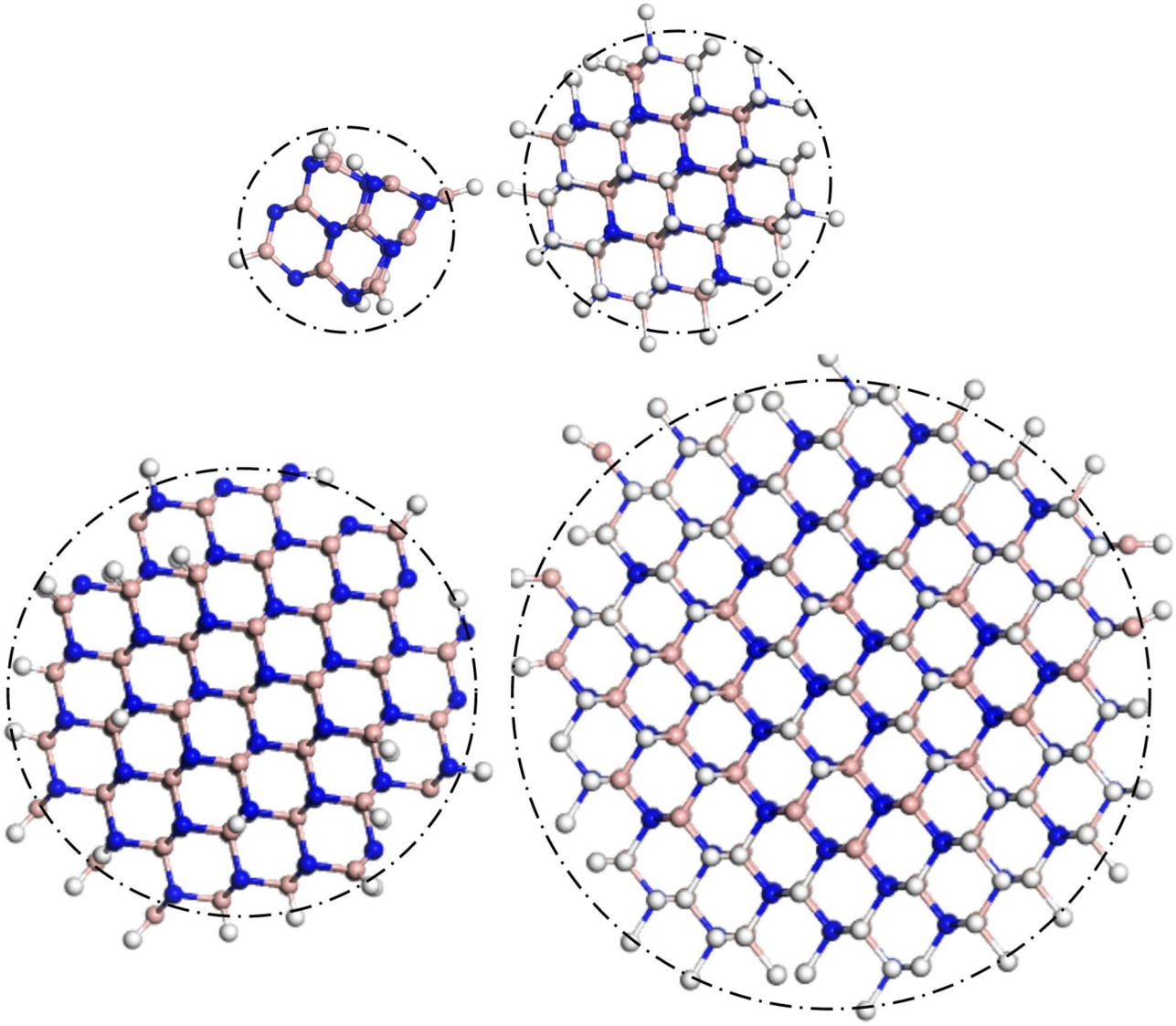

Fig. 1. Spherical BN nanoparticles with radii of 3, 5, 7, and 9 Å passivated by hydrogen atoms.

Property	This work	Other works	Reference	Comments
Binding Energy of Fe to BN (kJ/mol)	2.0–4.5	1.1–1.57 (nanotubes)	Wang et al.[43]	The binding energy in our work is higher due to the smaller size of nanoparticles, which enhances stability.
Interaction Distance (Å)	B-N: 1.43–1.48	B-N: 1.44–1.46	Bu et al.[44]	Our calculated B-N distances are consistent with experimental values for both –H and –OH terminated BN nanoparticles.
Drug Adsorption Energy (eV)	-0.6 to -1.4	-0.2 to -0.5	Permyakova et al.[45]	Our results show stronger adsorption energy, consistent with the enhanced reactivity of Fe-BNNCs compared to undoped BN.

Table 1. Comparison of DFT results with published experimental and theoretical data.

as the calculated frequency distribution reveals vibrational peaks at 629, 748, 891, 973, 1086, 1012, 1310, and 1580 cm-1, indicative of their characteristic vibrational modes.

Figure 3 visually represents the alterations in energy gap of (BN)-H and (BN)-OH nanoparticles. The energy gap of BN boron nitride nanoparticles stands as a critical parameter significantly influencing their electronic and optical characteristics. Notably, as the radius of BN nanoparticles escalates from 3 to 9 Å, a discernible diminishing trend unfolds in the energy gap. This reduction in the energy gap with increasing size is a prevalent phenomenon in nanomaterials, attributable to quantum confinement effects[52]. With the expansion of the nanocrystal size, electronic states tend to become more dispersed, culminating in a diminished energy demand to transition an electron from the valence band to the conduction band.

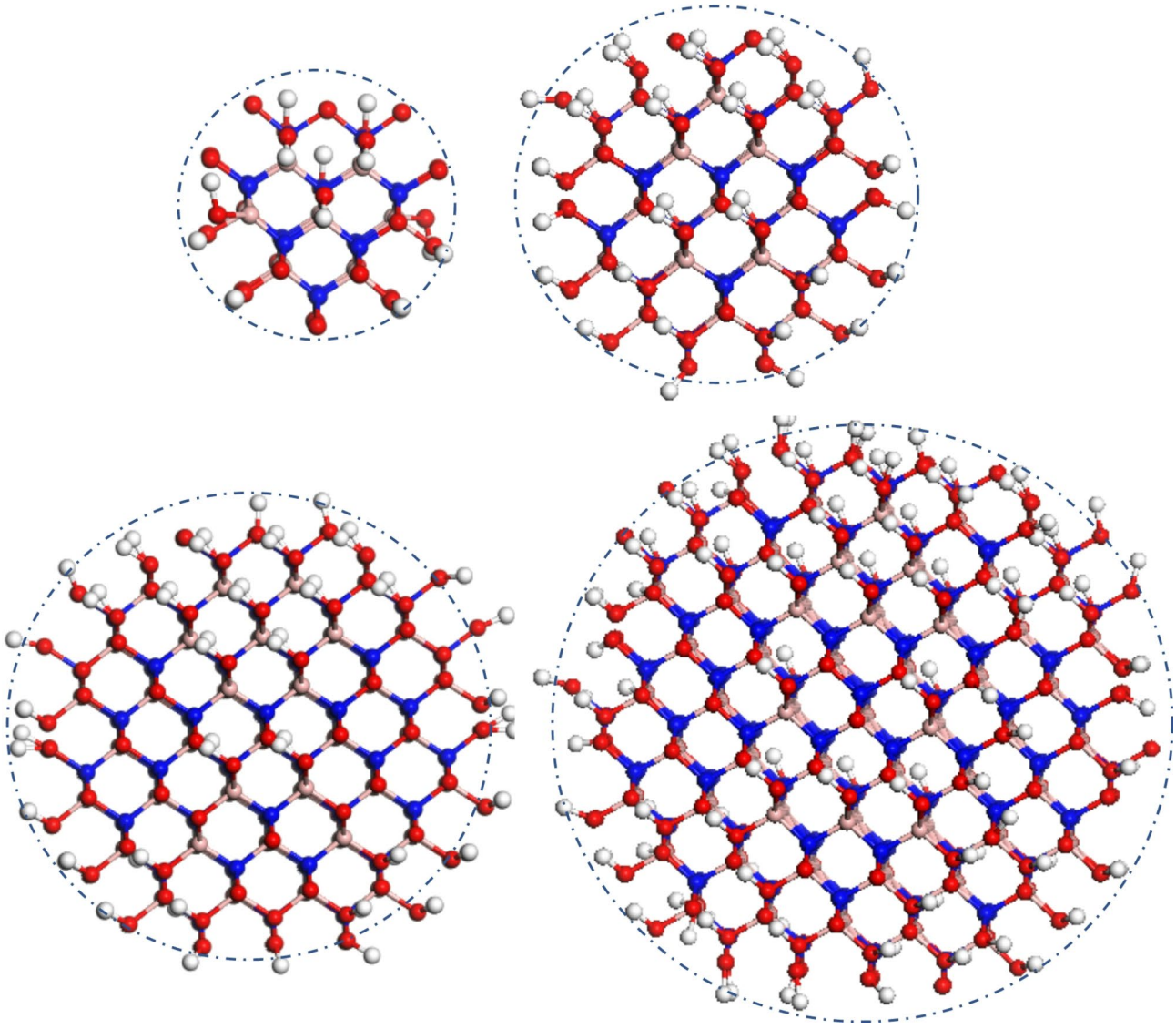

Fig. 2. Spherical BN nanoparticles with radii of 3, 5, 7, and 9 Å functionalized by -OH.

Moreover, research indicates that the energy gap of BN nanoparticles functionalized with hydrogen (-H) bonds surpasses that of hydroxyl (-OH) groups. Surface functionalization, by influencing surface states and charge transfer mechanisms, plays a pivotal role in reshaping the electronic structure of nanomaterials. The heightened energy gap observed in -H-passivated nanoparticles may be ascribed to the robust bonding between hydrogen and the BN surface, effectively curbing free charges and escalating the band gap in comparison to their -OH-passivated counterparts. The variation in the energy gap of BN nanoparticles spans a range from 4 to 2 eV, portraying how surface modifications can be leveraged to induce changes in energy gap values, serving as a foundation for diverse molecule absorption processes.

The functionalization of boron nitride nanomaterials can accentuate their properties and expand their applications. Metal-doped BN nanostructures exhibit promises as drug carriers, showcasing enhanced adsorption energy for anti-cancer drugs like gemcitabine[53]. Also, molecular adsorption on BN nanosheets can instigate structural alterations, energy elevation, and heightened adsorption efficiency[54]. Transition metal atoms can chemisorb on BN nanotubes, displaying distinct binding energies contingent on the metal type. Metals such as Sc, Ti, Ni, Pd, and Pt exhibit high binding energies exceeding 1 eV, while V, Fe, and Co manifest average couplings ranging from 0.62 to 0.92 eV[55]. Metal adsorption can engender impurity states within the band gap of pristine BN nanotubes, narrowing the gap and often yielding non-zero magnetic moments. These insights underscore how the functionalization of BN nanoparticles with iron clusters can enhance surface properties conducive to drug adsorption.

Figures 4 and 5 showcase Fe_{15} nanoclusters adsorbed on the surfaces of (BN)-H and (BN)-OH nanoparticles, denoted as (BN)-H@Fe_{15} and (BN)-OH@Fe_{15}, respectively. The Fe_{15} nanocluster exhibits a formation energy of -2.16 eV/atom, underscoring its stability, and features frequency peaks at 86, 159, 183, 276, and 365 cm^{-1}, aligning with experimental and theoretical findings[56]. Possessing Oh symmetry, the Fe_{15} nanocluster's Fe-

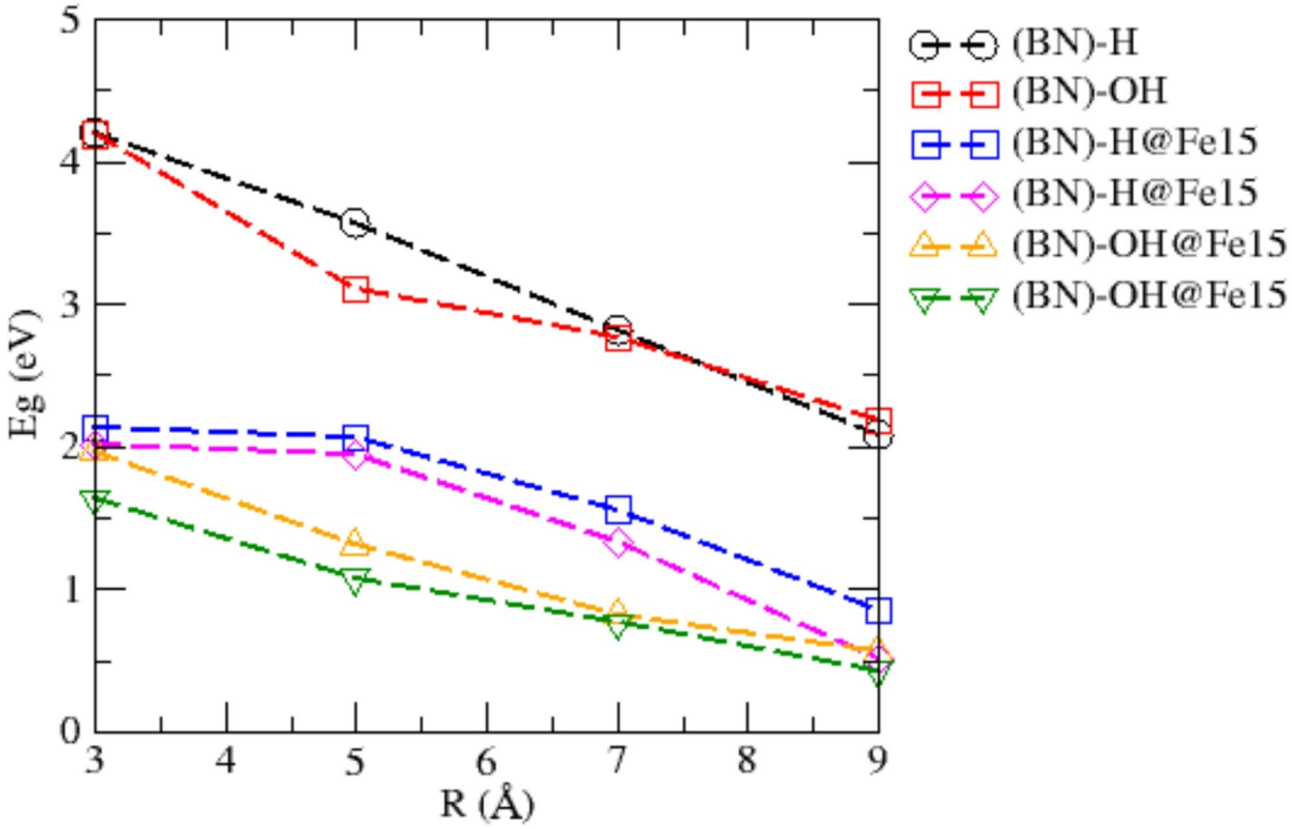

Fig. 3. Energy gap changes of functionalized and surface modified nanostructures with Fe_{15} nanocluster.

Fe bond lengths range between 2.5 and 2.7 Å, with a dipole moment near 4.3 Debye. Its adsorption on BN nanoparticles can augment surface polarization, subsequently heightening electrostatic interactions facilitating drug binding.

In Fig. 4, for the interaction of a (BN)-H nanocrystal with a radius of approximately 3 Å, the Fe_{15} nanocluster fractures, establishing robust bonds between iron atoms and the nanocrystal surface. The diminutive radius, around 3 Å, results in deformations in the (BN)-H nanocrystal, with B-Fe and N-Fe bonds generating a binding energy of roughly − 4.15 eV, indicative of a potent covalent bond. Analogously, akin behavior manifests in (BN)-OH nanoparticles with a 3 Å radius. The binding energy of the Fe_{15} nanocluster to the 3 Å (BN)-OH nanocrystal approximates − 4.5 eV, about 0.4 eV higher than the (BN)-H@Fe_{15} structure. B-Fe, N-Fe, and O-Fe bond lengths measure 1.95, 1.98, and 1.99 Å, respectively.

Figure 6 depicts the adsorption energy of the Fe_{15} nanocluster on (BN)-H and (BN)-OH nanoparticles. Notably, as nanocrystal radius expands, a consistent decline in binding energy transpires for both passivation types, indicating weaker interactions with the Fe_{15} cluster in larger nanoparticles, possibly influenced by surface alterations, electronic structure shifts, or steric effects with size increase. The persistent higher binding energy for passivated BN-OH nanoparticles compared to passivated BN-H nanoparticles implies that hydroxyl group passivation engenders stronger Fe_{15} cluster binding than hydrogen passivated BN nanoparticles. This discrepancy hints that hydroxyl groups enhance interaction with the Fe_{15} cluster, potentially due to robust chemical bonds or specific nanocluster surface configurations.

The distinct trends observed between passivated BN-H and BN-OH nanoparticles underscore the pivotal role of surface chemistry in dictating nanomaterial-cluster interaction strength, mirroring reported behavior for various studied structures. As particle size enlarges, absorption energy diminishes while maintaining near structural symmetry in the nanocluster, suggesting that iron nanoparticle amalgamation with BN nanoparticles can yield a coherent, reproducible structure with specific symmetry, where appropriate binding energy assures atomic clusters attachment to nanoparticles.

As per the insights from Fig. 3, the introduction of Fe_{15} nanoclusters can notably alter the energy gap of nanoparticles. While the energy gap of (BN)-H@Fe_{15} and (BN)-OH@Fe_{15} structures diminishes with increasing nanoparticle size, there exists a slightly higher energy gap for the hydrogen passivated states. The magnetic nature of iron nanoclusters leads to polarization of states with varying spins, resulting in the formation of spin-up and spin-down energy gaps. The discrepancy between the spin gaps of upper and lower states typically ranges between 0.2 and 0.5 eV for both hydrogen and hydroxyl surface coverages, exhibiting a relatively analogous behavior between H and –OH surface passivation scenarios.

In the following, we will examine the absorption of anastrozole (AN) molecules on (BN)-H, (BN)-OH, (BN)-H@Fe_{15}, and (BN)-OH@Fe_{15} nanoparticles, focusing specifically on the absorption details concerning

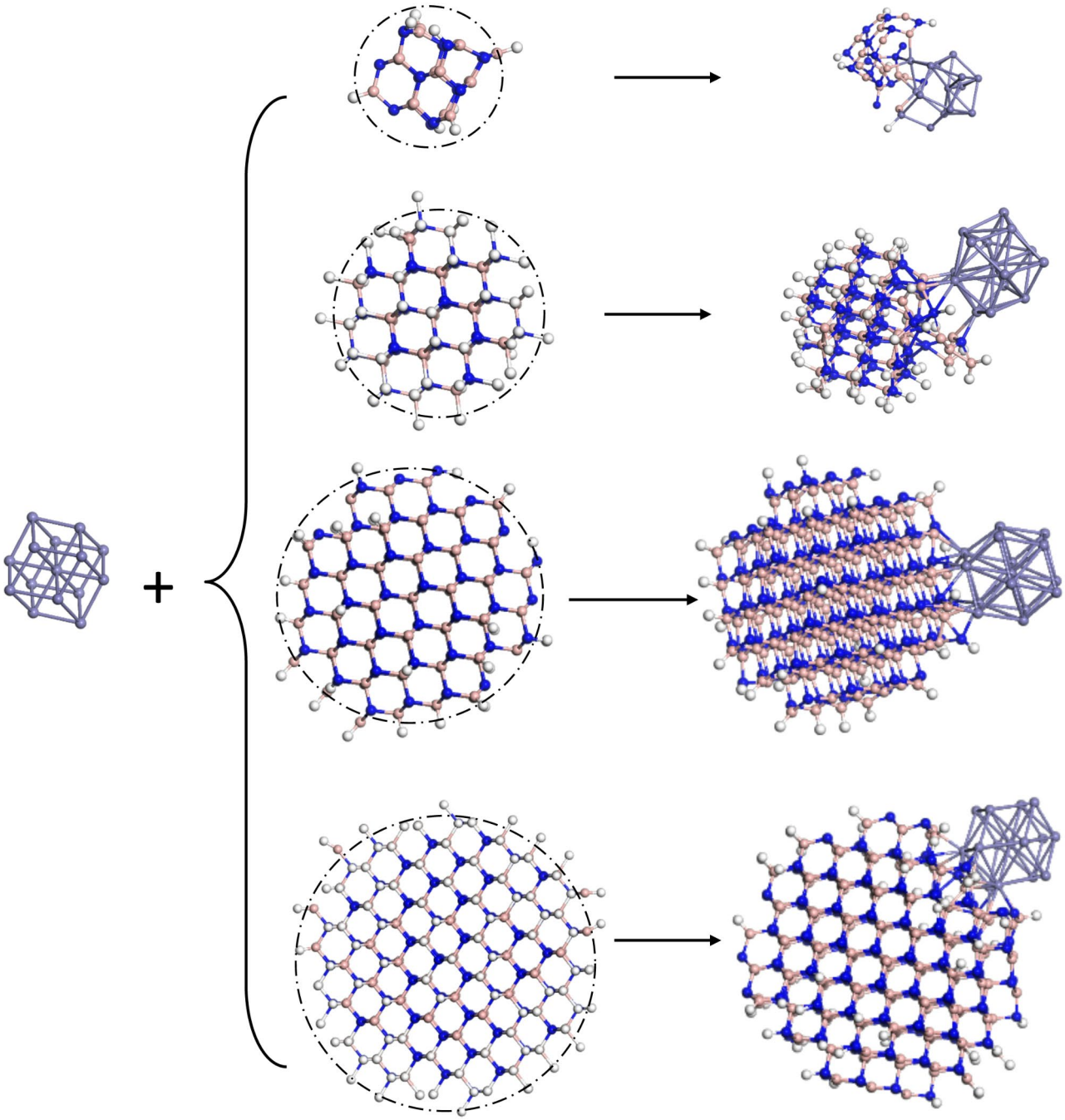

Fig. 4. Surface modified (BN)-H with iron nanoclusters of Fe_{15}.

nanocrystal structures with dimensions of 9 Å. Figure 7 illustrates the molecular structure of anastrozole and its interactions with the (BN)-H and (BN)-OH nanoparticles. Anastrozole belongs to a class of drugs known as aromatase inhibitors[56]. Chemically, anastrozole features a molecular structure comprising two primary carbon rings linked by single bonds, forming a stable and rigid framework. Additionally, multiple nitrogen atoms within the structure of anastrozole engage in bonding interactions with carbon atoms, contributing to the characteristic aromatic ring system of the molecule. The positioning of hydrogen atoms in anastrozole is also crucial; these hydrogen atoms attach to both nitrogen and carbon atoms, facilitating interactions such as hydrogen bonding, especially between hydrogen and nitrogen atoms. This bonding arrangement enhances the overall stability and structural integrity of the molecule[57]. Overall, the chemical structure of anastrozole, with interconnected carbon rings, nitrogen atoms participating in bonding interactions, and hydrogen atoms forming hydrogen bonds, underscores its unique composition as an aromatase inhibitor drug. The presence of nitrogen and the aromatic ring system in anastrozole is pivotal for its medicinal activity and its mechanism of action in inhibiting aromatase enzymes.

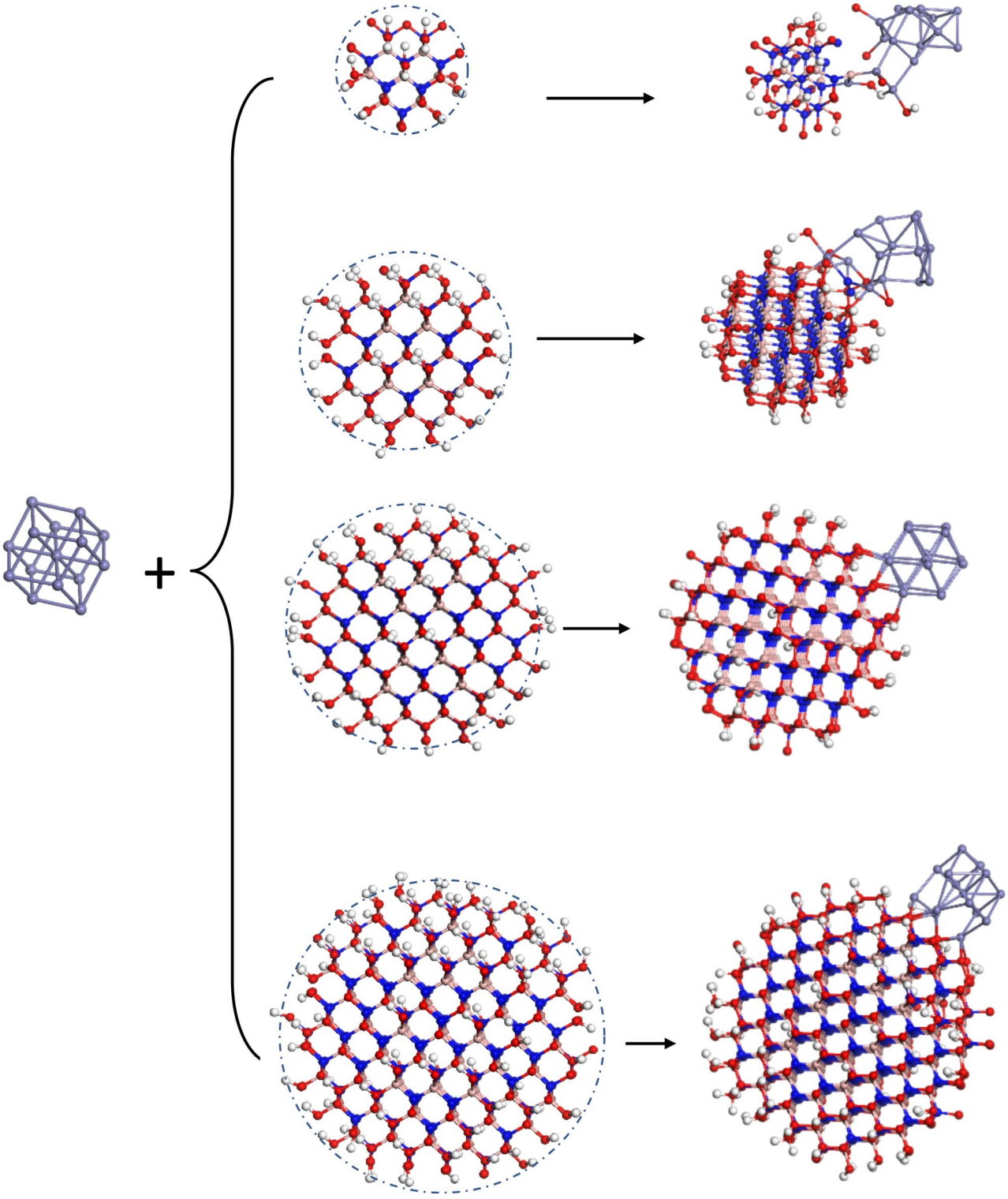

Fig. 5. Surface modified (BN)-OH with iron nanoclusters of Fe_{15}.

As depicted in Fig. 7, anastrozole is physically absorbed on the surface of (BN)-H and (BN)-OH nanoparticles, indicating the absence of an established covalent bond between the molecule and the surface in physical absorption. In the subfigure, the red circles on the molecule represent hydrogen interactions, while the green circles signify electrostatic interactions with the nanocrystal surface. It is evident from the figure that the interaction of anastrozole with the (BN)-H surface is predominantly influenced by hydrogen interactions, particularly from the hexagonal carbon ring side. The minimum distance between the anastrozole molecule and the surface is approximately 1.8 Å, with a charge transfer of about − 0.08e to the anastrozole surface.

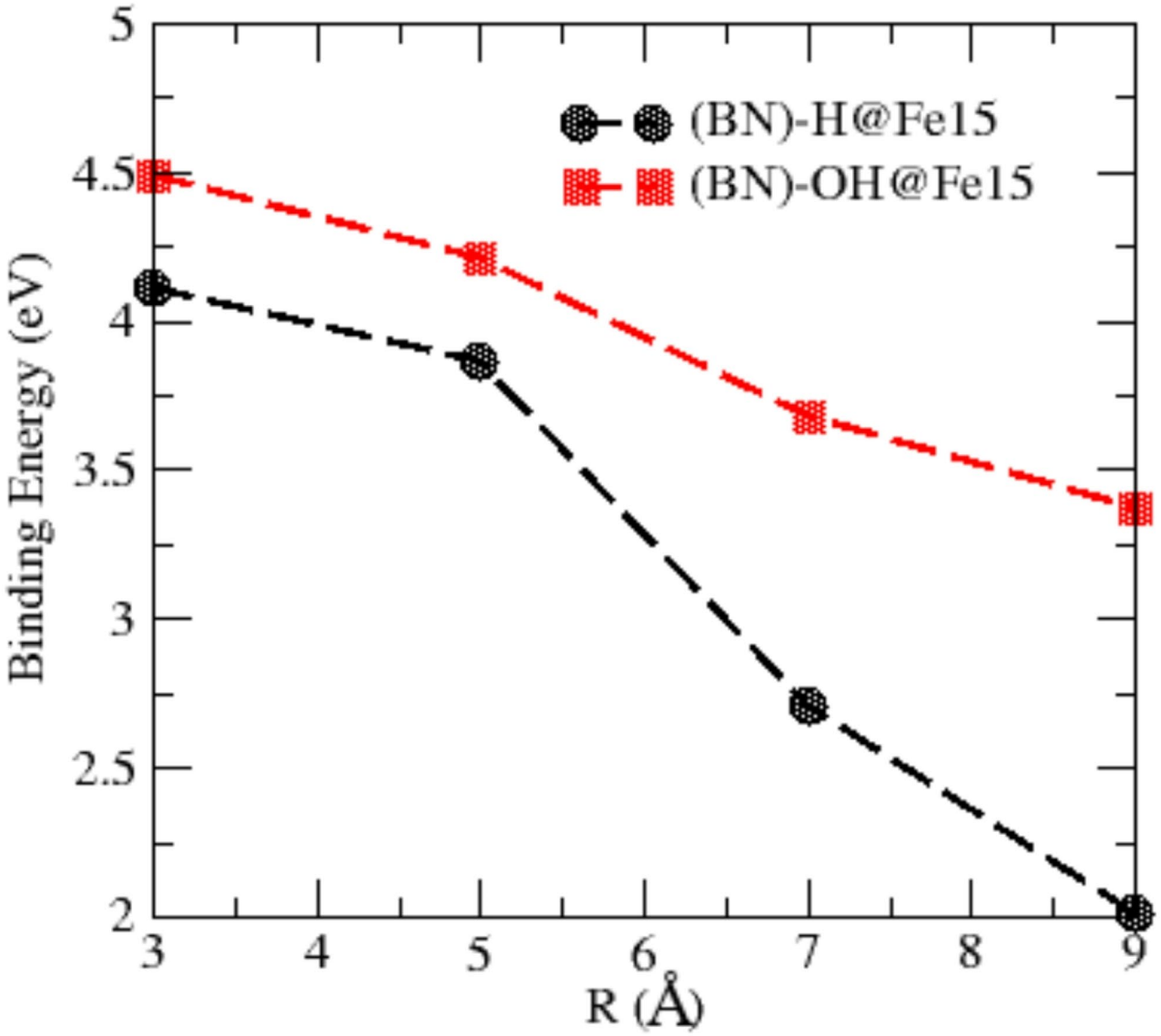

Fig. 6. Binding energy of iron nanoclusters on the surface of (BN)-H and (BN)-OH nanoparticles.

Figure 8 displays the adsorption energy of anastrozole for absorption on (BN)-H nanoparticles of varying radii. The figure indicates that the absorption energy on smaller nanoparticles is higher, and as the size of the nanoparticles increases, the absorption energy decreases. The range of anastrozole adsorption energy on (BN)-H nanoparticles is approximately 0.64 to 0.83 eV, whereas this value significantly differs for adsorption on nanoparticles coated with -OH. The range of changes in the adsorption energy on the (BN)-OH surface ranges from 0.87 to 1 eV depending on the nanoparticle size. These observations suggest that the adsorption energy on the (BN)-OH surface is less influenced by changes in radius and is more reliant on surface characteristics. The distance between the anastrozole molecule and the surface in the lowest energy state is about 1.68 Å. The interaction configuration of anastrozole with (BN)-OH reveals that, in addition to hydrogen interaction, the electrostatic interaction is also intensified. In such scenarios, the increase in adsorption energy can be attributed to the heightened electrostatic interaction of anastrozole with the (BN)-OH surface.

Figure 9 illustrates the interaction configuration of anastrozole with (BN)-H@Fe_{15}@AN and (BN)-OH@Fe_{15}@AN. In both cases, the absorption energy has increased with the presence of iron nanoclusters on the surface of the BN nanoparticles. For instance, in the (BN)-H@Fe_{15}@AN state with a radius of 9 Å, the absorption energy has risen to 1.3 eV. Similarly, in the (BN)-OH@Fe_{15}@AN structure, an increase of approximately 0.5 eV has been observed consistently across all cases. Despite the heightened absorption energy due to the presence of iron nanoclusters, the absorption energy still decreases with increasing size. Subfigure 9 depicts the placement of the Anastrozole molecule in proximity to the iron nanocluster. The created polarization results in an electrostatic interaction between the Anastrozole molecule and the iron nanocluster, as well as the BN surface, leading to an increase in the binding energy of the drug to the complex. The figure highlights the roles

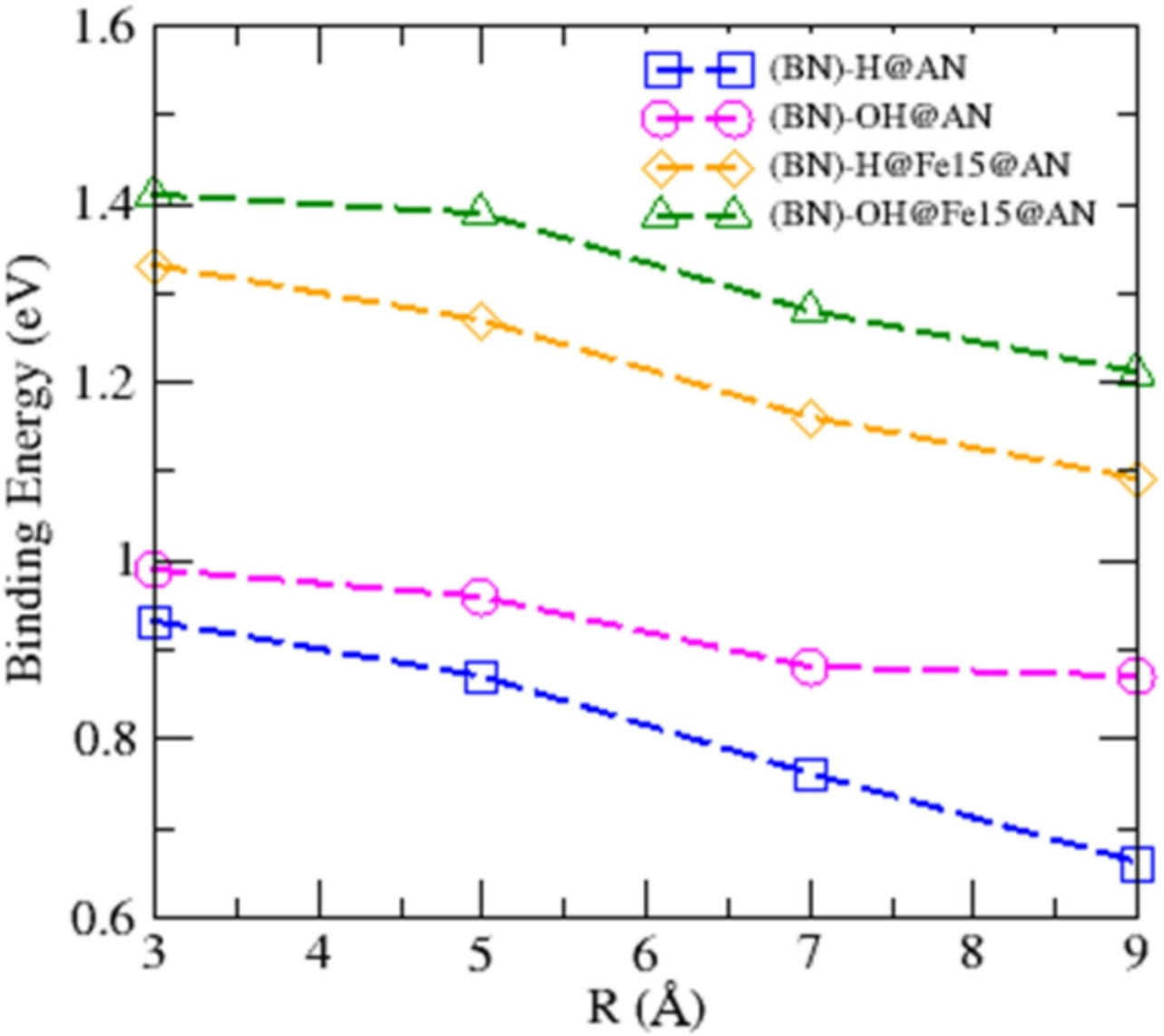

Fig. 7. illustrates the adsorption energy of anastrozole (AN) on the surfaces of (BN)-H, (BN)-OH, (BN)-H@Fe_{15}, and (BN)-OH@Fe_{15} nanoparticles.

of hydrogen and electrostatic interactions on Anastrozole atoms interacting with (BN)-H@Fe_{15} and (BN)-OH@Fe_{15}, demonstrating that electrostatic interaction predominates in areas with iron nanoclusters.

Detailing the electronic structure of the discussed complexes can be instrumental in elucidating experimental results. Figure 10 showcases the quantum levels of (BN)-H and (BN)-OH nanoparticles, as well as @Fe_{15} (BN)-H and (BN)-OH@Fe_{15} in the presence of the anastrozole molecule. The interaction post absorption of the iron nanocluster significantly alters the electronic structure of the substances in their pure states. Notably, changes in the vicinity of the HOMO and LUMO levels indicate effective charge transfer between the drug and the nanocrystal-nanocluster complex, leading to alterations in the energy gap width. Figure 11 illustrates changes in the energy gap, revealing a decrease with increasing nanocrystal radius. Moreover, the addition of iron nanoclusters further diminishes the energy gap. In this context, OH-coated nanoparticles exhibit a smaller gap due to the magnetic polarization induced by the iron clusters, resulting in an energy gap in both spin-polarized (up, down) states. Figure 12 presents the HOMO and LUMO wave functions for the 9Å state, demonstrating the chemically active spatial positions. The distribution of wave functions highlights that as the molecule approaches the surface, HOMO and LUMO states form near the Anastrozole drug, predominantly distributed on the surface, indicating charge polarization near the surface and electronic structure rearrangement. Table 2 details the degree of polarization of the discussed structures. With an increase in iron nanoclusters on the surface of (BN)-H nanoparticles, the degree of polarization rises from 22.87 to 55.19 Debye, while for (BN)-OH nanoparticles, it increases from 68.73 to 76.98 Debye. This increase underscores that the addition of iron clusters significantly enhances the surface polarization of nanoparticles. Furthermore, the dipole moment of (BN)-OH nanoparticles surpasses that of (BN)-H nanoparticles in all cases, attributed to the presence of -OH bonds and their intrinsic

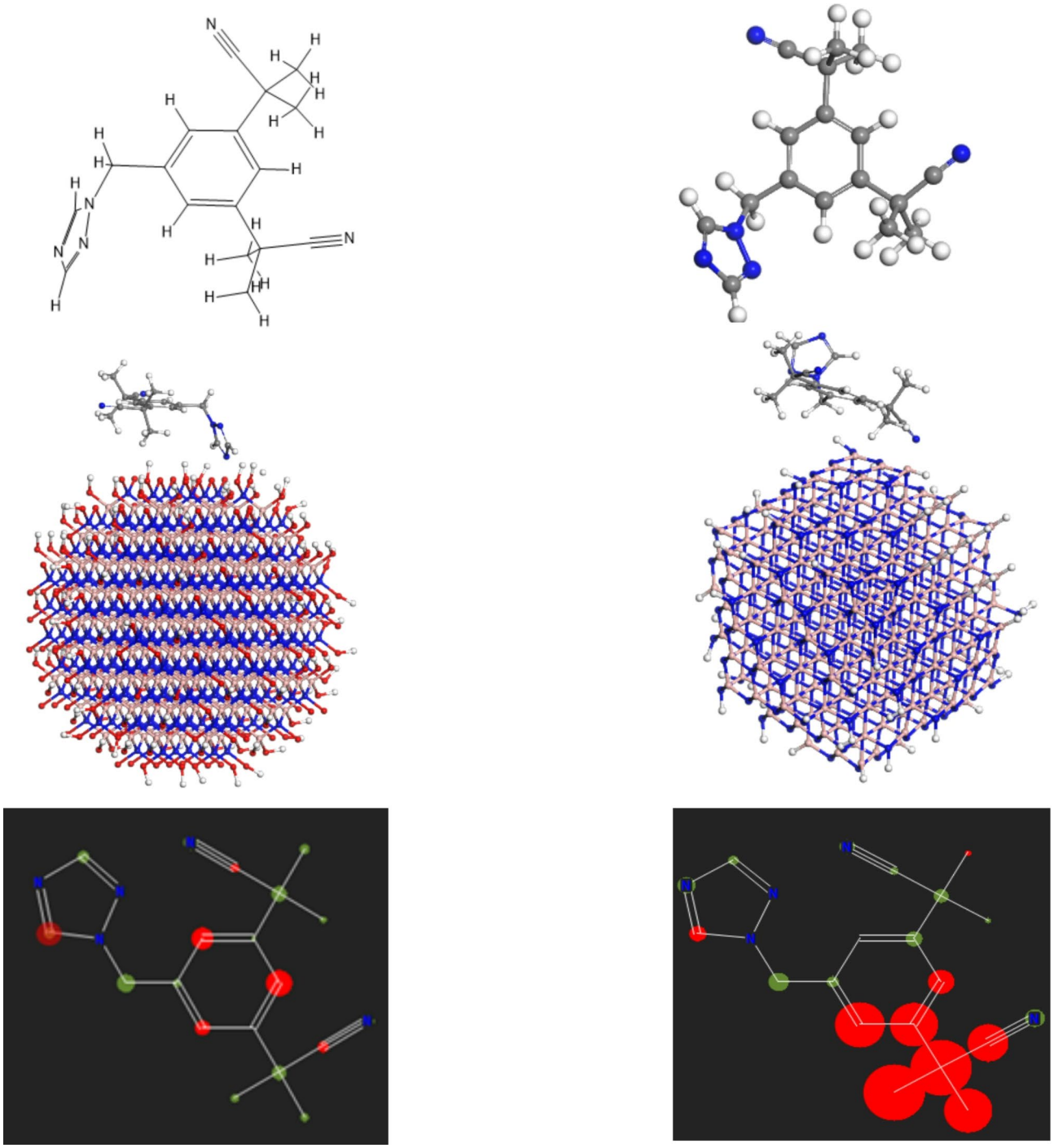

Fig. 8. displays the structural representation of the Anastrozole molecule, along with (BN)-H and (BN)-OH nanoparticles interacting with the molecule. It illustrates the interaction configuration of various positions of the molecule with the surface, where red circles represent hydrogen interactions and green circles signify electrostatic interactions.

polarization. Additionally, the electric dipole value of the complex slightly increases with the addition of AN molecules.

The dipole generated on the nanocrystal surface can establish an internal electric field, influencing the movement of energy levels, particularly the HOMO and LUMO levels, as depicted in Fig. 11; Table 2. Finally, Fig. 13 displays the density of states of the discussed structures, showcasing significant changes at the energy gap edges and in the position and intensity of peaks. These alterations underscore the profound interaction of the AN molecule with the nanocrystal structure, surface modification by iron nanoclusters, and the minor changes in the nanocrystal structure's interaction with AN.

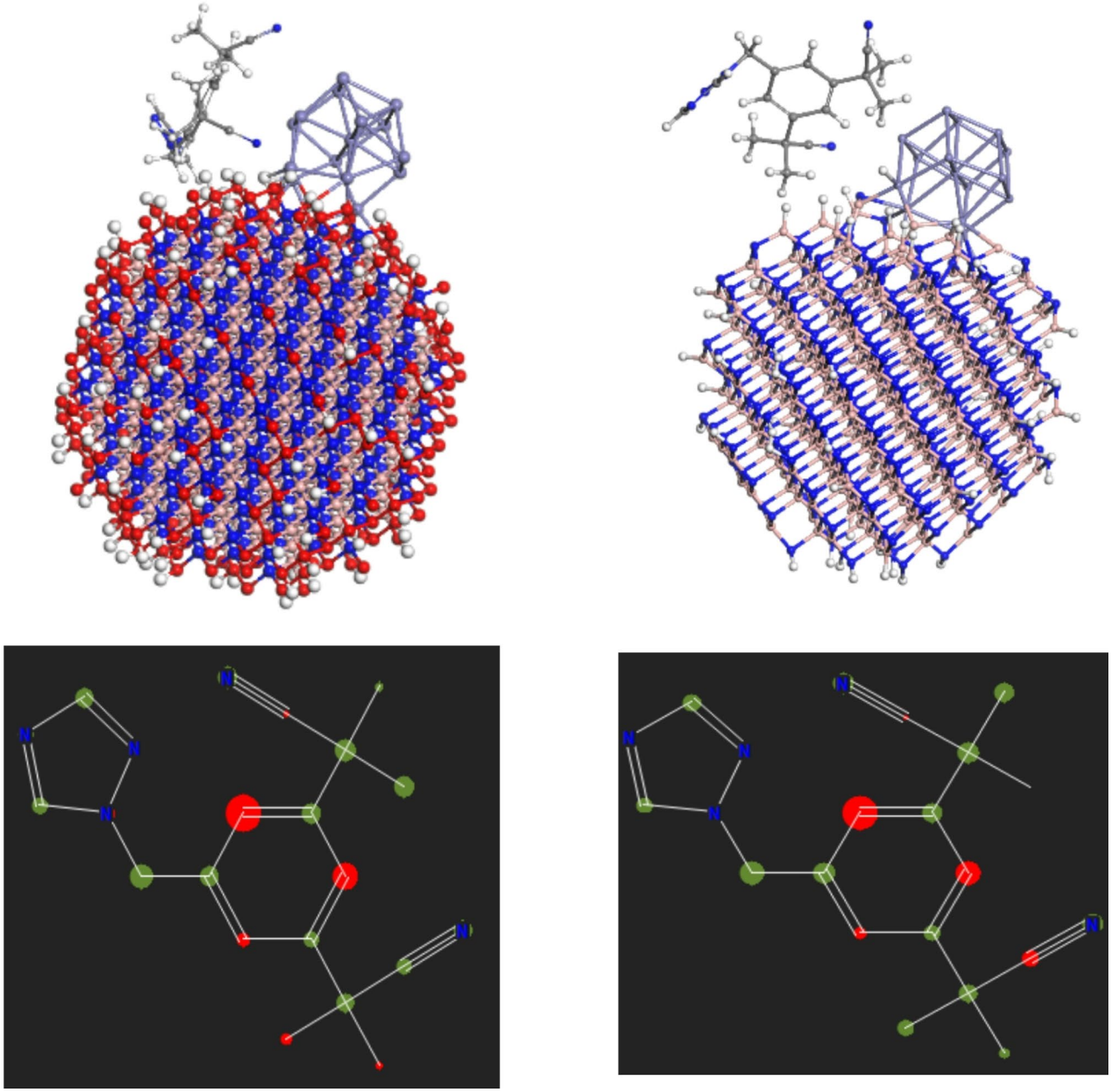

Fig. 9. (BN)-H@Fe_{15} and (BN)-OH@Fe_{15} nanoparticles interacting with anastrozol molecule.

Figure 14 depicts the optical absorption spectrum of the aforementioned states. The optical absorption spectrum serves as a valuable criterion for identifying compounds generated on an experimental scale, with the intensity and position of peaks subject to variations based on the nature of interactions. Both (BN)-H and (BN)-OH nanoparticles exhibit multiple peaks within the 250 to 600 nm range, with specific key peaks aiding in their distinction. Notably, the (BN)-H nanocrystal features a peak in the absorption range of 280 to 300 nm, while this peak shifts to 350 nm in the case of (BN)-OH. Moreover, a prominent peak of higher intensity emerges in the 430 to 460 nm range for (BN)-H nanoparticles, which relocates to 450 to 490 nm for (BN)-OH nanoparticles. Upon AN integration, there are slight alterations in peak intensity and position, notably a red shift of approximately 50 to 60 nm around peak of 450 nm compared to the pure nanocrystal states. Overall, surface modification of nanoparticles with the Fe_{15} cluster induces a substantial change in the absorption spectrum, leading to main peak shifts into the 550–630 nm region. The absorption of AN further red-shifts these peaks to some extent, indicating a reduction in the energy gap of the nanostructures and a decreased energy requirement for inter-band transitions.

For further studies we investigate the role of pH and temperature on the binding energy of the AN adsorbed on BNNP with radius of 9Å on different –H and –OH functionalized surfaces. The Fig. 15a illustrates the binding energies of AN on two different structures: iron-functionalized boron nitride nanoparticles ($H_{210}B_{269}N_{276}$@

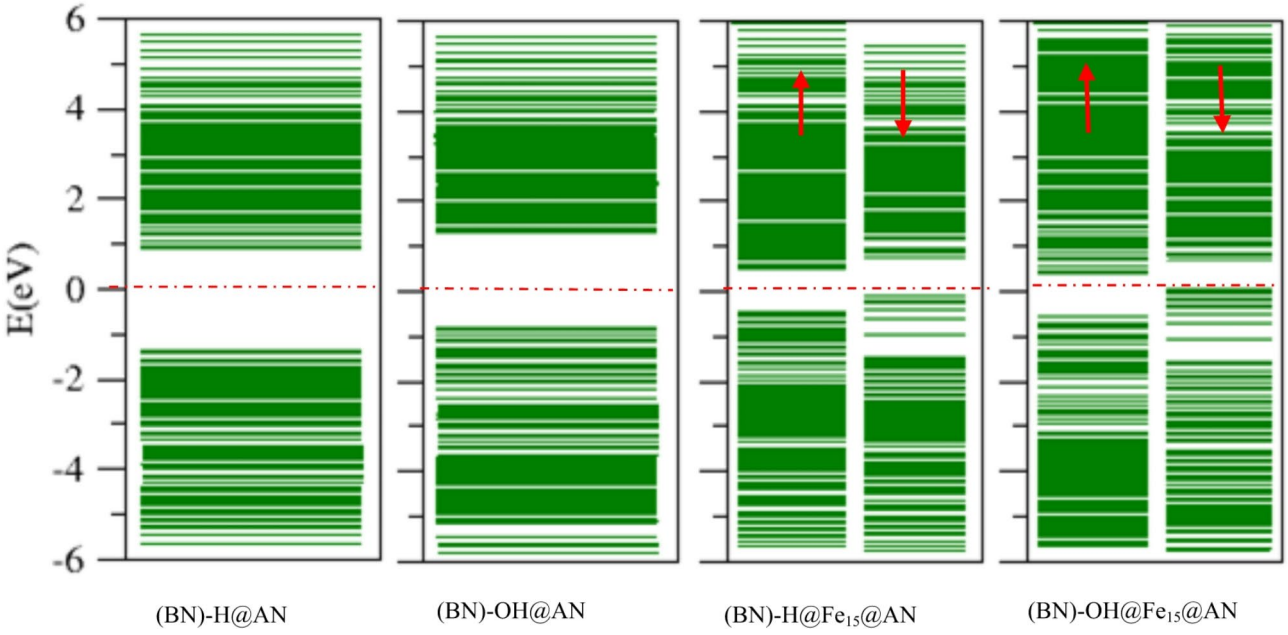

Fig. 10. The electronic structure of nanostructures exhibiting maximum stability upon adsorption of AN.

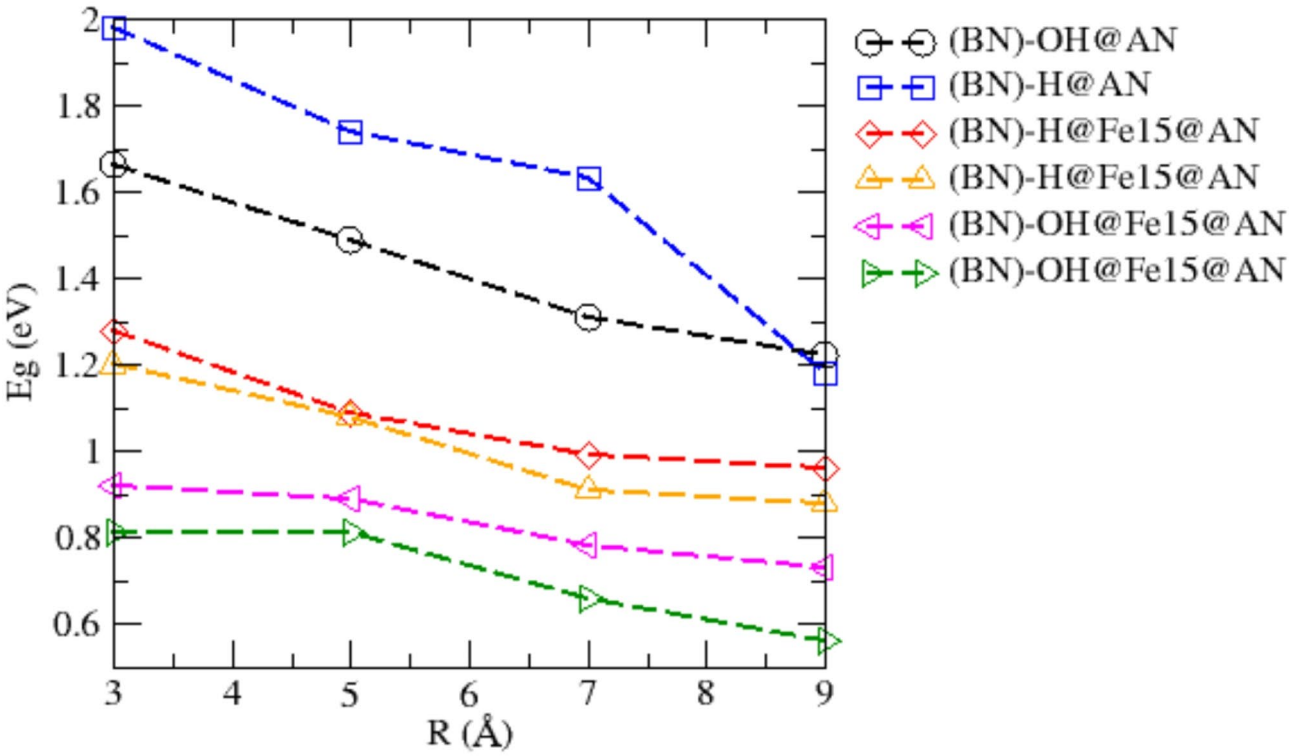

Fig. 11. The alterations in the energy gap of the nanostructures following the introduction of AN.

Fe_{15}@AN) and non-functionalized boron nitride nanoparticles ($H_{210}B_{269}N_{276}$@AN) across various pH states. In the neutral state, the adsorption energy for the iron-functionalized structure is significantly higher at 1.254 eV, while the non-functionalized structure shows a lower binding energy of 0.76 eV. This suggests that the presence of the iron cluster enhances the interaction between AN and the BN nanoparticles, indicating a stronger affinity for the drug. In slightly acidic conditions ($H_{220}B_{269}N_{276}$), the trend continues, with the binding energy for the iron-functionalized structure at 1.12 eV, compared to 0.68 eV for the non-functionalized counterpart. This further confirms that the iron cluster maintains its role in facilitating stronger adsorption, even as the pH shifts

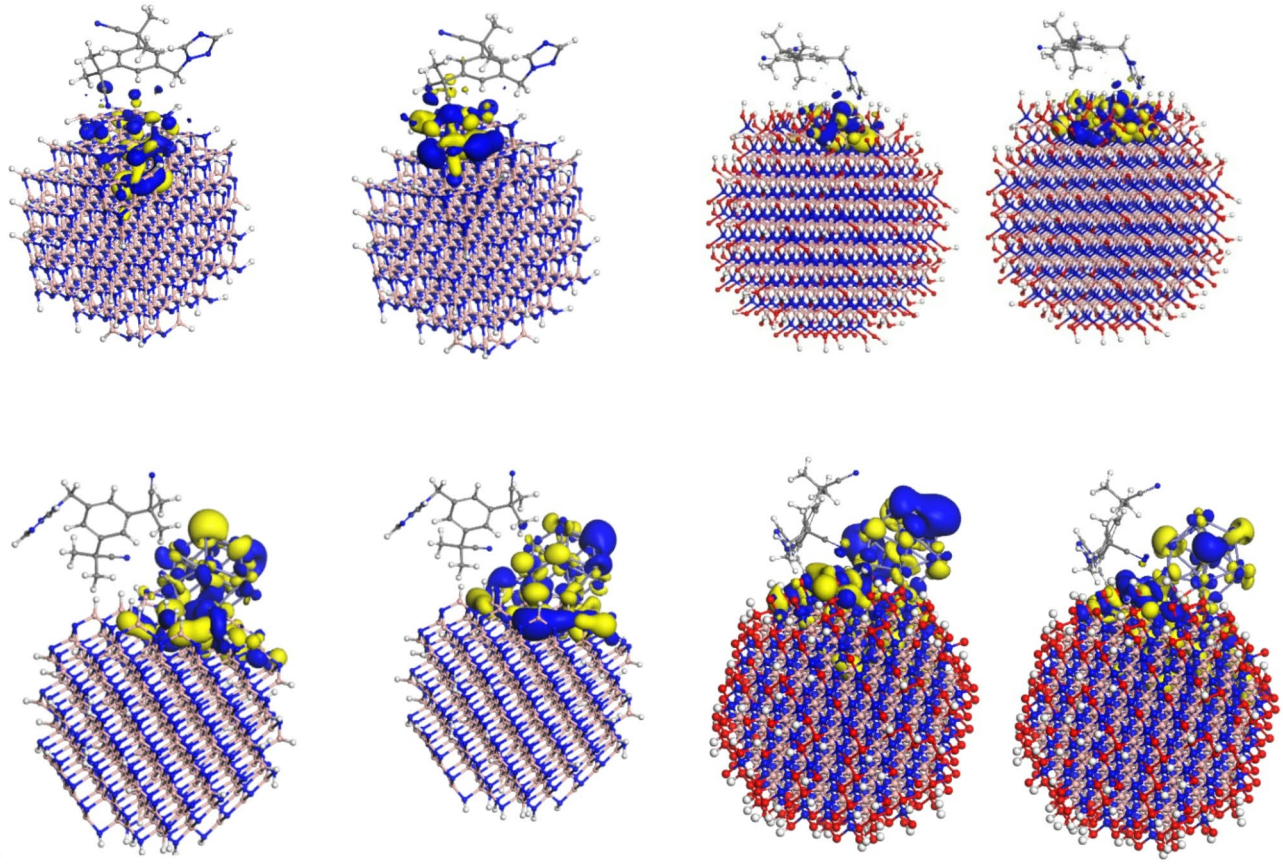

Fig. 12. the HOMO and LUMO wave functions in AN@Fe_{15}@(BN)-H, AN@Fe_{15}@(BN)-OH, AN@(BN)-H structures, and AN@(BN)-OH structures.

Property (R = 9 Å)	(BN)-H	(BN)-OH	(BN)-H@Fe15	(BN)-OH@Fe15	(BN)-H@Fe15@AN	(BN)-OH@Fe15@AN
E_{HOMO}/eV	-6.23	-5.825	-4.61(-3.75)	-3.67(-3.255)	-2.66(-2.073)	-2.375(-1.7)
E_{LUMO}/eV	-4.15	-3.635	-4.435(-3.925)	-3.11(-2.825)	-1.7(-1.193)	-1.645(-1.14)
E_g/eV	2.08	2.19	0.86(0.51)	0.56(0.43)	0.96(0.88)	0.73(0.56)
μ_D/*Debye*	22.87	68.73	55.19	76.98	59.32	78.11
E_F/eV	-5.19	-4.73	-4.18	-3.39(-3.04)	-2.18(-1.63)	-2.01(-1.42)

Table 2. Calculated HOMO energies (E_{HOMO}/eV), LUMO energies (E_{LUMO}/eV), dipole moment (μ_D/Debye), and energy gap (E_g/eV) for the pure and complexes of (BN)-H and (BN)-OH nanoparticles (with radius of 9 Å) functionalized with Fe_{15} nanocluster and AN molecule.

slightly. The consistent increase in binding energy under these conditions highlights the potential benefits of utilizing iron clusters in enhancing drug-carrier interactions. In alkaline conditions ($H_{190}B_{269}N_{276}$), the binding energy for the iron-functionalized structure is 1.09 eV, showing a slight decrease from the acidic state but remaining higher than the non-functionalized structure, which has a binding energy of 0.55 eV. This observation indicates that while the effectiveness of iron clusters may diminish slightly in alkaline environments, they still provide a superior interaction for AN compared to the non-functionalized BN. Overall, the figure emphasizes the advantageous role of iron functionalization in improving the adsorption characteristics of BN nanoparticles for drug delivery applications. The analysis reveals that the dipole moment of the iron-functionalized boron nitride structures exhibits an increase in acidic environments and a decrease in alkaline conditions, showcasing a direct correlation with the binding energy of Anastrozole (AN). In slightly acidic conditions, the higher dipole moments—ranging from 59.32 to 63.17 Debye suggest enhanced polarity, which likely facilitates stronger interactions with the polar drug molecule, resulting in increased adsorption energy. Conversely, in alkaline environments, the dipole moments drop, aligning with the observed decrease in binding energy. This relationship indicates that as the polarity of the functionalized structures changes with pH, so too does their ability to effectively adsorb AN, underscoring the importance of both dipole moment and environmental pH in influencing adsorption dynamics.

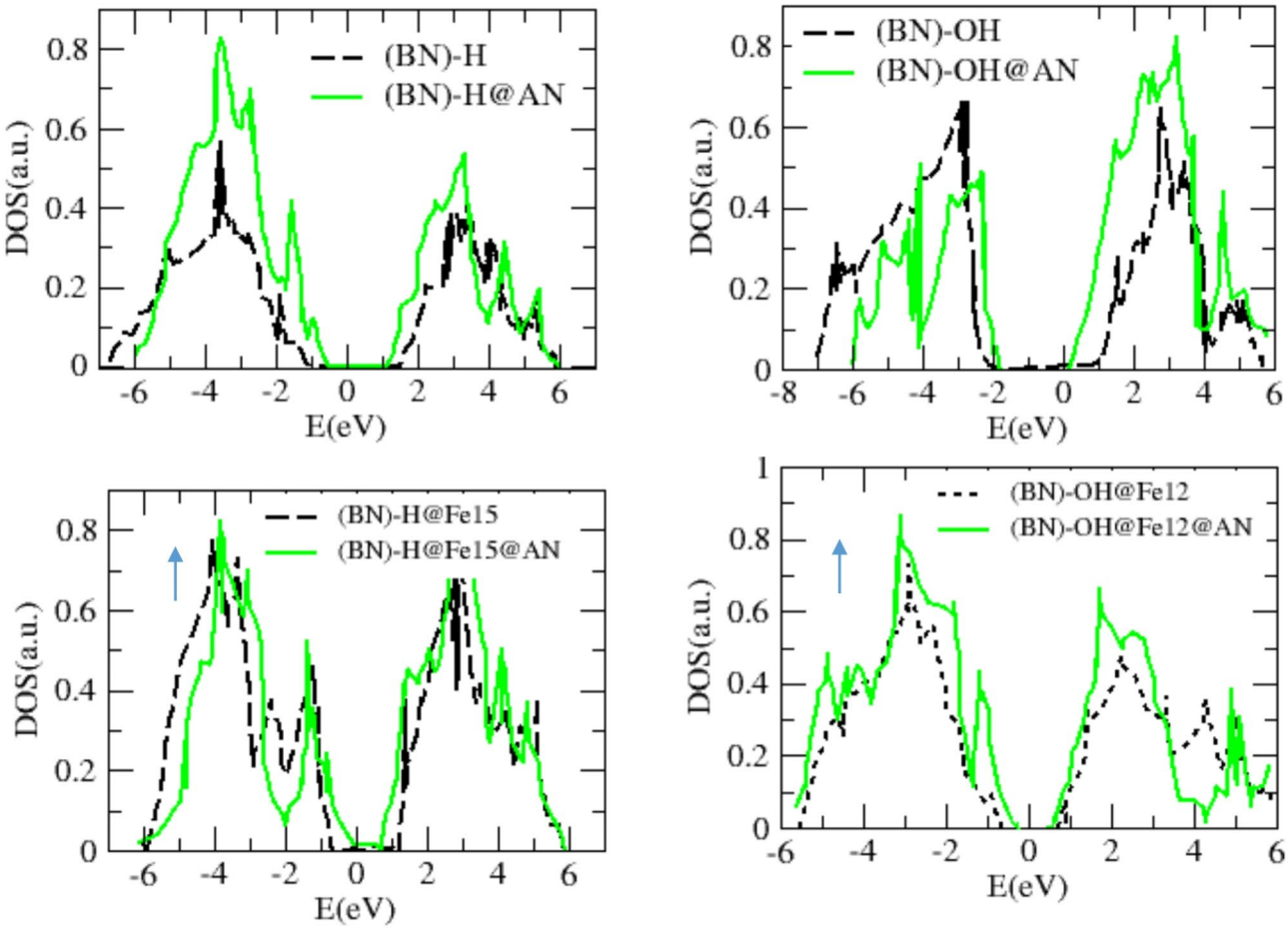

Fig. 13. illustrates the density of states structure of the absorbing configurations of the AN molecule.

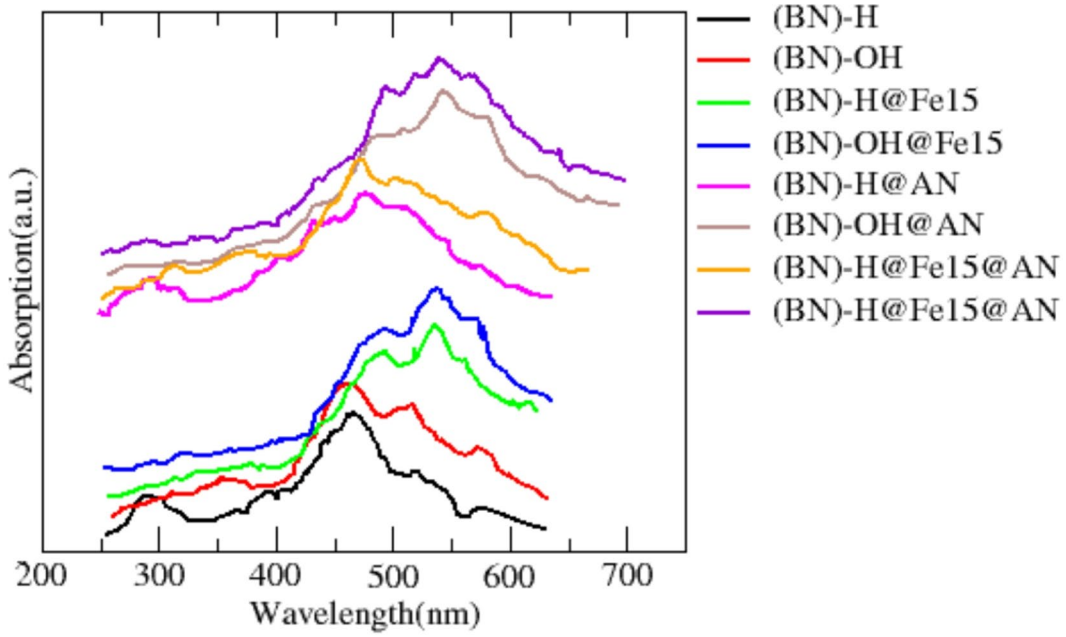

Fig. 14. Optical absorption spectrum for pristine states and post-adsorption of iron nanoclusters and the AN molecule on the nanocrystal structure.

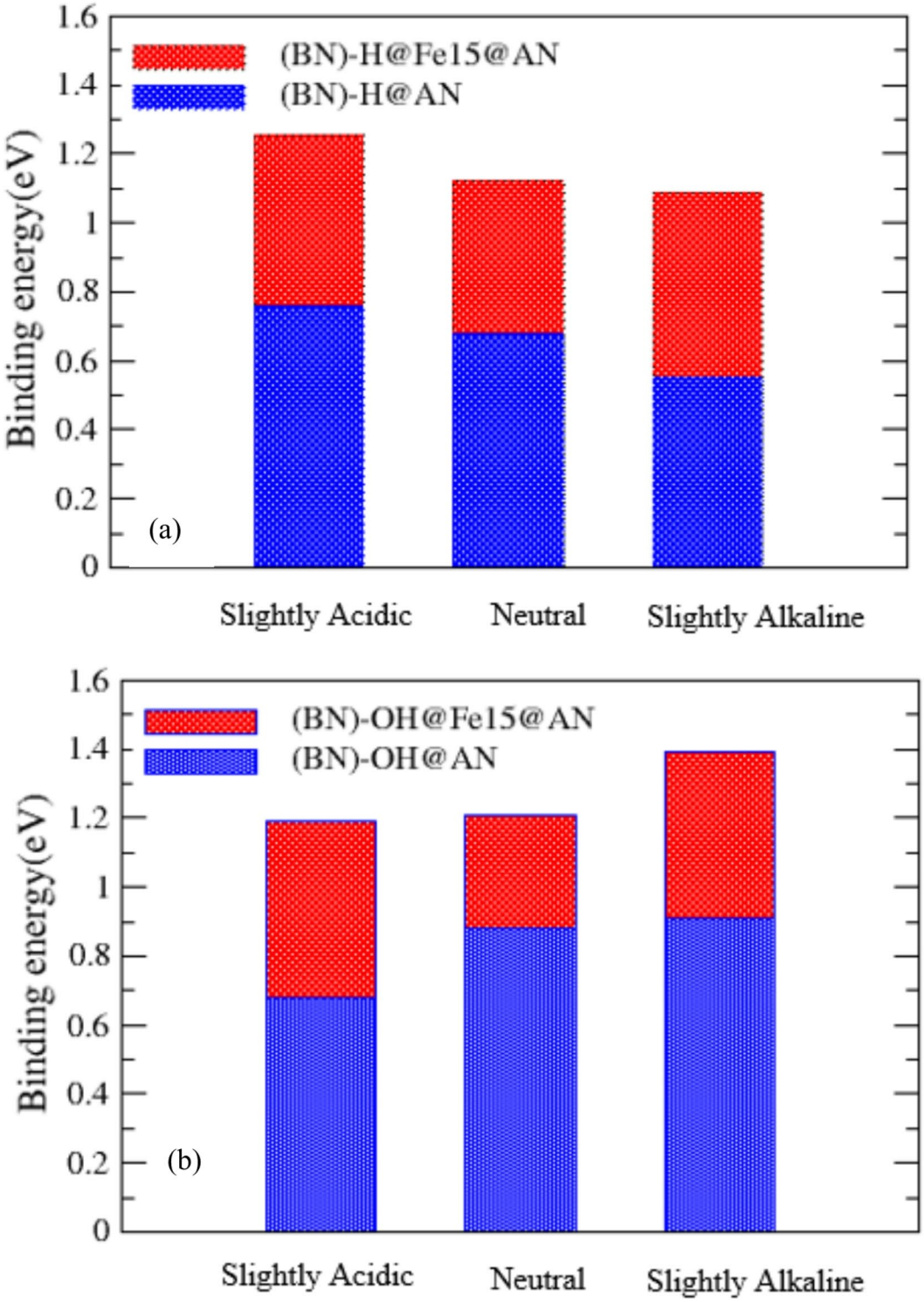

Fig. 15. The binding energy of AN molecule to (**a**) –H (**b**) -OH terminated BNNP and BNNP@Fe_{15} nanoparticles.

The Fig. 15b presents the binding energies of AN on -OH terminated boron nitride nanoparticles, the data reveals that the iron-functionalized structures consistently exhibit higher binding energies compared to their non-functionalized counterparts across different pH states. For example, in the neutral state, the binding energy for $H_{100}B_{249}N_{276}O_{228}@Fe_{15}@AN$ is 1.19 eV, while the non-functionalized $H_{100}B_{249}N_{276}O_{228}@AN$ has a significantly lower adsorption energy of 0.68 eV. This trend indicates that the presence of the iron cluster enhances the affinity of AN for the -OH terminated BN structures.

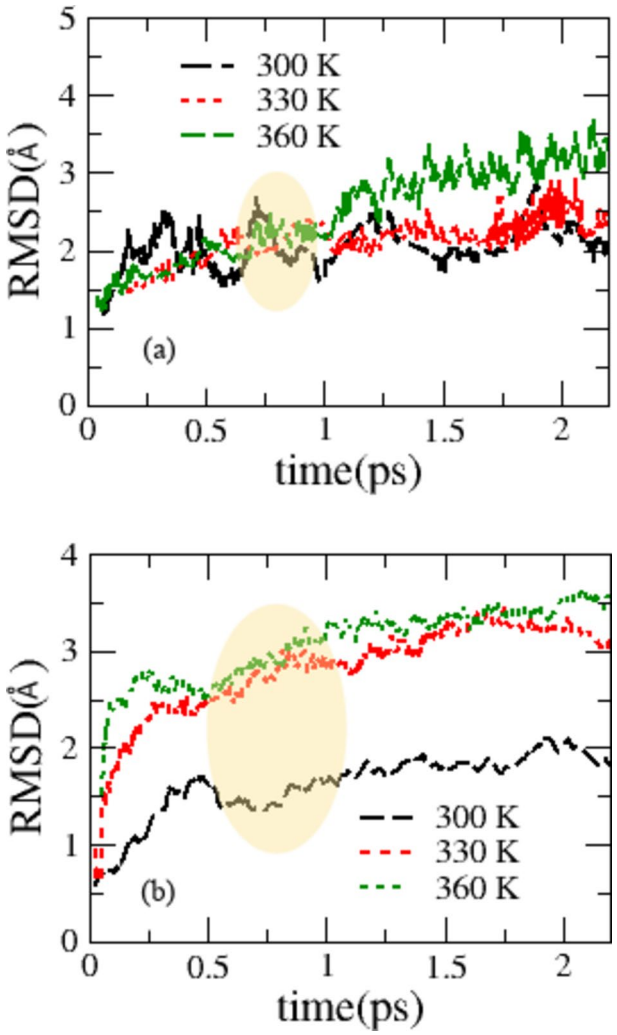

Fig. 16. The RMSD of AN molecule to (**a**) –H (**b**) -OH terminated BNNP and BNNP@Fe_{15} nanoparticles.

As the pH shifts, the iron-functionalized structures continue to demonstrate strong binding characteristics. The binding energy for the $H_{110}B_{249}N_{276}O_{228}$@$Fe_{15}$@AN (slightly acidic) is 1.21 eV, and it increases further to 1.39 eV for $H_{90}B_{249}N_{276}O_{228}$@$Fe_{15}$@AN (slightly alkaline). In contrast, the respective non-functionalized structures show lower binding energies of 0.88 eV and 0.91 eV. In addition to binding energy, the dipole moments of the structures provide further insight into their adsorption behavior. The iron-functionalized structures exhibit higher dipole moments, ranging from 67.19 to 79.16 Debye, compared to the non-functionalized structures, which show dipole moments between 33.28 and 41.12 Debye. This increased polarity likely contributes to the stronger adsorption of AN, as the enhanced dipole moments facilitate better interactions with the polar drug molecule. Overall, the data underscores the significant role of iron clusters in not only improving the binding energy of AN on -OH terminated BN nanoparticles but also enhancing the structural polarity, which positively influences adsorption dynamics.

The Fig. 16a and b illustrate the root mean square deviation (RMSD) of Anastrozole (AN) adsorbed on –H and -OH terminated boron nitride nanoparticles functionalized with iron clusters at different temperatures (300, 330, and 360 K) over a duration of 2 ps. The data is presented with distinct lines for each temperature, with the RMSD values showing a relatively stable trend throughout the simulation. Notably, the highlighted region indicates a correlation between temperature and AN binding energy, revealing that as the temperature increases from 300 K to 360 K, the binding energy of the configuration decreases, with values of 0.42, -0.27, and − 0.18 eV, for –H and 0.31, -0.17, and − 0.08 eV for –OH terminated BNNP ($R = 9$ Å). This trend suggests that higher temperatures may lead to increased molecular motion, resulting in weaker interactions between AN and the functionalized BN nanoparticles, thereby decreasing the adsorption energy. Overall, the figure underscores the impact of temperature on the stability of the adsorption configuration, highlighting the importance of thermal effects in adsorption phenomena.

Conclusion

(BN)-H and (BN)-OH nanoparticles, enhanced with iron nanoclusters, were utilized for anastrozole absorption. The electrical and optical attributes of free nanocrystal structures within a radius range of 3 to 9 Å were computed using density functional theory. The findings highlight the dependency of anastrozole interaction on particle dimensions and nanoparticle surface properties. Nanoparticles coated with -H bonds exhibit more stable structures compared to those coated with -OH bonds, although their electronic characteristics, such as the energy gap, show relatively close values. Surface modifications with iron nanoclusters can significantly alter various nanocrystal properties, including the energy gap, density of states, and dipole moment. Through surface polarization adjustments, iron nanoclusters enhance the electrostatic interaction between the nanocrystal surface and the AN molecule, leading to an increase in the binding energy of anastrozole to the nanocrystal surface. The optical absorption spectrum serves as an evaluative indicator that can elucidate the substance's interaction state. When anastrozole is introduced to the surface of pristine nanoparticles with differing -H and -OH coverages, notable disparities in the absorption spectrum peaks are observed. However, post-surface modification with Fe_{15} nanoclusters, a red shift in the peak of the optical absorption spectrum occurs, signaling a substantial alteration in the nanoparticles' electronic state.

Data availability

All data generated or analysed during this study are included in this published article.

Received: 7 November 2024; Accepted: 3 March 2025
Published online: 13 March 2025

References

1. Weng, Q., Wang, X., Wang, X., Bando, Y. & Golberg, D. Functionalized hexagonal boron nitride nanomaterials: Emerging properties and applications. *Chem. Soc. Rev.* **45**(14), 3989–4012 (2016).
2. Lima, D. M., Chinellato, A. C. & Champeau, M. Boron nitride-based nanocomposite hydrogels: Preparation, properties and applications. *Soft Matter* **17**(17), 4475–4488 (2021).
3. Terrones, M. et al. Pure and doped boron nitride nanotubes. *Mater. today* **10**(5), 30–38 (2007).
4. Li, X. M. et al. Substitutional doping of BN nanotube by transition metal: A density functional theory simulation. *Comput. Theor. Chem.* **964**(1–3), 199–206 (2011).
5. Merlo, A., Mokkapati, V. R. S. S., Pandit, S. & Mijakovic, I. Boron nitride nanomaterials: Biocompatibility and bio-applications. *Biomater. Sci.* **6**(9), 2298–2311 (2018).
6. Wang, W. et al. Fe_3O_4 nanoparticle-coated boron nitride nanospheres: Synthesis, magnetic property, and biocompatibility study. *Ceram. Int.* **43**(8), 6371–6376 (2017).
7. Tabtimsai, C. et al. Ibuprofen adsorption and detection of pristine, Fe–, Ni–, and Pt–doped boron nitride nanotubes: A DFT investigation. *J. Mol. Gr. Modell.* **126**, 108654 (2024).
8. Hesabi, M. & Behjatmanesh-Ardakani, R. Interaction between anti-cancer drug hydroxycarbamide and boron nitride nanotube: A long-range corrected DFT study. *Comput. Theor. Chem.* **1117**, 61–80 (2017).
9. Kawsar, S. M., Munia, N. S., Saha, S. & Ozeki, Y. In silico pharmacokinetics, molecular docking and molecular dynamics simulation studies of nucleoside analogs for drug discovery-a mini review. *Mini Rev. Med. Chem.* **24**(11), 1070–1088 (2024).
10. Tedesco, D., Pistolozzi, M., Zanasi, R. & Bertucci, C. Characterization of the species-dependent ketoprofen/albumin binding modes by induced CD spectroscopy and TD-DFT calculations. *J. Pharm. Biomed. Anal.* **112**, 176–180 (2015).
11. Lumachi, F., Brunello, A., Maruzzo, M., Basso, U. & Mm Basso, S. Treatment of estrogen receptor-positive breast cancer. *Curr. Med. Chem.* **20**(5), 596–604 (2013).
12. Gonçalves, R. F., Martins, J. T., Duarte, C. M., Vicente, A. A. & Pinheiro, A. C. Advances in nutraceutical delivery systems: From formulation design for bioavailability enhancement to efficacy and safety evaluation. *Trends Food Sci. Technol.* **78**, 270–291 (2018).
13. Manzari, M. T. et al. Targeted drug delivery strategies for precision medicines. *Nat. Rev. Mater.* **6**(4), 351–370 (2021).
14. Javan, M. B. Magnetic properties of $Mg_{12}O_{12}$ nanocage doped with transition metal atoms (Mn, Fe, Co and Ni): DFT study. *J. Magn. Magn. Mater.* **385**, 138–144 (2015).
15. Javan, M. B., Soltani, A., Azmoodeh, Z., Abdolahi, N. & Gholami, N. A DFT study on the interaction between 5-fluorouracil and $B_{12}N_{12}$ nanocluster. *RSC Adv.* **6**(106), 104513–104521 (2016).
16. Soltani, A., Sousaraei, A., Javan, M. B., Eskandari, M. & Balakheyli, H. Electronic and optical properties of 5-AVA-functionalized BN nanoclusters: A DFT study. *New J. Chem.* **40**(8), 7018–7026 (2016).
17. Cao, Y. et al. Investigations of adsorption behavior and anti-cancer activity of curcumin on pure and platinum-functionalized $B_{12}N_{12}$ nanocages. *J. Mol. Liq.* **334**, 116516 (2021).
18. Munir, I. et al. Therapeutic potential of graphyne as a new drug-delivery system for daunorubicin to treat cancer: A DFT study. *J. Mol. Liq.* **336**, 116327 (2021).
19. Javan, M. B. & Orimi, R. L. Electric field and phosphorus doping roles on the electronic and optical properties of SiC Nanocrystals: First principles study. *J. Comput. Theor. Nanosci.* **12**(6), 1023–1029 (2015).
20. Javan, M. B. Small cobalt clusters encapsulated inside $Si_{30}C_{30}$ nanocages: Electronic and magnetic properties. *J. Mol. Model.* **20**, 1–13 (2014).
21. Adekoya, O. C., Adekoya, G. J., Sadiku, E. R., Hamam, Y. & Ray, S. S. Application of DFT calculations in designing polymer-based drug delivery systems: An overview. *Pharmaceutics* **14**(9), 1972 (2022).
22. Rahman, H., Hossain, M. R. & Ferdous, T. The recent advancement of low-dimensional nanostructured materials for drug delivery and drug sensing application: A brief review. *J. Mol. Liq.* **320**, 114427 (2020).
23. Mane, S. K. B., Shaishta, N. & Manjunatha, G. Biocompatibility, toxicity evaluations, environmental and health impact of hexagonal boron nitride. In *Hexagonal Boron Nitride* 613–636 (Elsevier, 2024). https://doi.org/10.1016/B978-0-443-18843-5.00002-1.
24. Manaia, E. B. et al. Physicochemical characterization of drug nanocarriers. *Int. J. Nanomed.* **12**, 4991–5011. https://doi.org/10.2147/IJN.S133832 (2017).
25. Dobson, J. Magnetic nanoparticles for drug delivery. *Drug Dev. Res.* **67**(1), 55–60 (2006).
26. Mody, V. V. et al. Magnetic nanoparticle drug delivery systems for targeting tumor. *Appl. Nanosci.* **4**, 385–392 (2014).
27. Elzoghby, A. O. et al. Lactoferrin, a multi-functional glycoprotein: Active therapeutic, drug nanocarrier & targeting ligand. *Biomaterials* **263**, 120355 (2020).
28. Wu, L., Zhang, J. & Watanabe, W. Physical and chemical stability of drug nanoparticles. *Adv. Drug Deliv. Rev.* **63**(6), 456–469 (2011).
29. Chertok, B. et al. Iron oxide nanoparticles as a drug delivery vehicle for MRI monitored magnetic targeting of brain tumors. *Biomaterials* **29**(4), 487–496 (2008).

30. Abdolahi, N. et al. Gold decorated $B_{12}N_{12}$ nanocluster as an effective sulfasalazine drug carrier: A theoretical investigation. *Phys. E Low-Dimens. Syst. Nanostruct.* **124**, 114296 (2020).
31. Maurya, A. et al. Drug delivery potential of γ-graphyne, 6, 6, 12-graphyne and γ-graphdiyne for 5-Fluorouracil: insights from DFT calculations. *Compos. Interfaces*, 1–21. https://doi.org/10.1080/09276440.2025.2460350 (2025).
32. Bechohra, L. L., Kurban, M., Medigue, N. E. H. & Kellou-Taïri, S. Drug delivery potential of carbon and boron nitride nanotubes: A DFT-D3 analysis of curcumin binding interactions. *Diamond Relat. Mater.* **149**, 111626 (2024).
33. Kurban, M., Polat, C., Serpedin, E. & Kurban, H. Enhancing the electronic properties of TiO_2 nanoparticles through carbon doping: An integrated DFTB and computer vision approach. *Comput. Mater. Sci.* **244**, 113248 (2024).
34. Balasubramani, S. G. et al. TURBOMOLE: Modular program suite for ab initio quantum-chemical and condensed-matter simulations. *J. Chem. Phys.* **152**(18), (2020).
35. Hourahine, B. et al. DFTB+, a software package for efficient approximate density functional theory based atomistic simulations. *J. Chem. Phys.* **152**(12), 124101 (2020).
36. Ozaki, T. Variationally optimized atomic orbitals for large-scale electronic structures. *Phys. Rev. B* **67**(15), 155108 (2003).
37. Weigend, F. Accurate Coulomb-fitting basis sets for H to Rn. *Phys. Chem. Chem. Phys.* **8**(9), 1057–1065 (2006).
38. Boys, S. F. & Bernardi, F. J. M. P. The calculation of small molecular interactions by the differences of separate total energies. Some procedures with reduced errors. *Mol. Phys.* **19**(4), 553–566 (1970).
39. Rasti, S. & Meyer, J. Importance of zero-point energy for crystalline ice phases: A comparison of force fields and density functional theory. *J. Chem. Phys.* **150**(23), 234504 (2019).
40. Wahiduzzaman, M. et al. DFTB parameters for the periodic table: part 1, electronic structure. *J. Chem. Theory Comput.* **9**(9), 4006–4017 (2013).
41. Leung, K. & Whaley, K. B. Surface relaxation in CdSe nanoparticles. *J. Chem. Phys.* **110**(22), 11012–11022 (1999).
42. Cui, Z., Oyer, A. J., Glover, A. J., Schniepp, H. C. & Adamson, D. H. Large scale thermal exfoliation and functionalization of Boron nitride. *Small* **10**(12), 2352–2355 (2014).
43. Wang, R. X., Zhang, D. J., Zhu, R. X. & Liu, C. B. Theoretical study of the adsorption of Pentachlorophenol on the pristine and Fe-doped Boron nitride nanotubes. *J. Mol. Model.* **20**, 1–6 (2014).
44. Bu, H. et al. The role of sp^2 and sp^3 hybridized bonds on the structural, mechanical, and electronic properties in a hard BN framework. *RSC Adv.* **9**(5), 2657–2665 (2019).
45. Permyakova, E. S. et al. Experimental and theoretical study of doxorubicin physicochemical interaction with BN (O) drug delivery nanocarriers. *J. Phys. Chem. C* **122**(46), 26409–26418 (2018).
46. Jin, W. et al. Surface functionalization of hexagonal Boron nitride and its effect on the structure and performance of composites. *Appl. Surf. Sci.* **270**, 561–571 (2013).
47. Yin, J. et al. Boron nitride nanostructures: fabrication, functionalization and applications. *Small* **12**(22), 2942–2968 (2016).
48. Gao, Z., Zhi, C., Bando, Y., Golberg, D. & Serizawa, T. Noncovalent functionalization of boron nitride nanotubes in aqueous media opens application roads in nanobiomedicine. *Nanobiomedicine* **1**, 7 (2014).
49. Amstad, E., Textor, M. & Reimhult, E. Stabilization and functionalization of iron oxide nanoparticles for biomedical applications. *Nanoscale* **3**(7), 2819–2843 (2011).
50. Wang, Y. et al. Effect of covalent functionalization on thermal transport across graphene–polymer interfaces. *J. Phys. Chem. C.* **119**(22), 12731–12738 (2015).
51. Liu, Z., Li, J. & Liu, X. Novel functionalized BN nanosheets/epoxy composites with advanced thermal conductivity and mechanical properties. *ACS Appl. Mater. Interfaces*. **12**(5), 6503–6515 (2020).
52. Borrelli, N. F., Hall, D. W., Holland, H. J. & Smith, D. W. Quantum confinement effects of semiconducting microcrystallites in glass. *J. Appl. Phys.* **61**(12), 5399–5409 (1987).
53. Bibi, S. et al. Investigation of the adsorption properties of gemcitabine anticancer drug with metal-doped Boron nitride fullerenes as a drug-delivery carrier: A DFT study. *RSC Adv.* **12**(5), 2873–2887 (2022).
54. Vatanparast, M. & Shariatinia, Z. Hexagonal Boron nitride nanosheet as novel drug delivery system for anticancer drugs: Insights from DFT calculations and molecular dynamics simulations. *J. Mol. Graph. Model.* **89**, 50–59 (2019).
55. Hassan, J. et al. h-BN nanosheets doped with transition metals for environmental remediation; A DFT approach and molecular docking analysis. *Mater. Sci. Eng. B* **272**, 115365 (2021).
56. Ratre, P. et al. Aromatase inhibitors for the treatment of breast cancer: A journey from the scratch. *Anti-Cancer Agents Med. Chem. (Formerly Curr. Med. Chemistry-Anti-Cancer Agents)* **20**(17), 1994–2004 (2020).
57. Song, X. et al. Design rules of hydrogen-bonded organic frameworks with high chemical and thermal stabilities. *J. Am. Chem. Soc.* **144**(24), 10663–10687 (2022).

Acknowledgements

The authors extend their appreciation to the Deanship of Scientific Research at King Khalid University for funding this work through a Large Group Research Project under grant number RGP 2/78/46.

Author contributions

M.J.A., A.F.W., and S.T. wrote the main manuscript text. A.A., M.M.A., and F.A. prepared Figs. 1, 2, 3, 4, 5, 6, 7, 8, 9, 10, 11, 12, 13 and 14. S.B.S., Y.B.M., and U.H. reviewed the manuscript.

Declarations

Competing interests

The authors declare no competing interests.

Additional information

Correspondence and requests for materials should be addressed to M.J.A.

Reprints and permissions information is available at www.nature.com/reprints.

Publisher's note Springer Nature remains neutral with regard to jurisdictional claims in published maps and institutional affiliations.